

Proton-Proton Bremsstrahlung Measurements at 20 MeV*

Derek W. Storm† and R. Heffner

Department of Physics, University of Washington, Seattle, Washington 98105

(Received 17 June 1971)

We have measured the proton-proton bremsstrahlung cross section, $d\sigma/d\Omega_1 d\Omega_2$, with 20-MeV incident proton energy, detecting coincident protons at 25° and at 30° on either side of the beam. In addition, we have determined the photon angular distributions, $d\sigma/d\Omega_1 d\Omega_2 d\theta_\gamma$. The value measured for $d\sigma/d\Omega_1 d\Omega_2$ for proton angles of 25° is $0.68 \pm 0.07 \mu\text{b}/\text{sr}^2$ while that for 30° is $0.69 \pm 0.07 \mu\text{b}/\text{sr}^2$. These results are for coplanar geometry and are determined from the data using the azimuthal angular dependence for the cross section predicted by Drechsel and Maximon. The results agree with the predictions of Marker and Signell, when Coulomb corrections are included.

I. INTRODUCTION

Considerable effort has been spent in measuring¹⁻³ and predicting⁴⁻⁸ cross sections for proton-proton bremsstrahlung (PPB). Because this cross section is calculable in terms of the well-understood electromagnetic interaction and the off-energy-shell (OES) matrix elements of the two-proton transition operator, one of the ultimate goals of the work has been to use PPB data to test various two-nucleon potentials. Several such potentials have been proposed which reproduce the two-proton elastic scattering fairly well. As theoretical calculations have progressed, however, it has become apparent that in order for PPB measurements to select among these potentials the experiments should be carried out with incident energies well in excess of about 100 MeV.⁵ This restriction arises from the fact that the PPB cross section is so low that the statistical uncertainty attained in an experiment of reasonable duration is at best about 5%, and this uncertainty is larger than the calculated differences in the cross section for the various potentials for incident energies below about 100 MeV. Furthermore, the photon energy should be at least $\frac{1}{2}$ to $\frac{3}{4}$ of the available energy, because, for the case of relatively low-energy photons, the PPB cross section can be determined directly from a knowledge of the elastic cross section. (One relevant expansion parameter, which must be much less than 1 for this prediction, is the ratio of the photon energy to the total available energy.⁸)

In spite of these limitations, however, measurements below 100 MeV are definitely useful. Before one can expect to be able to use PPB data to choose among the various potential models, the general theory must be tested against precise experimental results in a relatively model-independent energy region. To date, however, measurements below 100 MeV of about 10% or better accu-

racy have been published at only three energies, 99,¹ 61.7, and 64.4 MeV.^{2,5}

As mentioned above, it is desirable to have precise data for photon energies as large as possible. All the PPB experiments so far have involved the detection of both final-state protons at generally equal angles on either side of the beam; in only one measurement (Rothe, Koehler, and Thorndike³) was the photon detected as well. For all the other experiments the photon energy and angles were therefore determined kinematically from those of the protons. Hence, since the PPB cross section drops with increasing photon energy (decreasing proton angle), the majority of the data have been measured with equal proton angles of 30° or more.

The present experiment was performed at 20-MeV incident energy and achieved a precision of about 10% in the determination of $d\sigma/d\Omega_1 d\Omega_2$. Coincident final-state protons were detected at equal counter angles of 25 and 30°. In addition there was one run for which one counter was at 25° and the other at 27.5°. For 20-MeV incident energy and 25° proton angles the photon energy is about $\frac{3}{4}$ of the incident c.m. energy so the OES effects are relevant. In addition the Coulomb corrections to the theoretical cross section at 20 MeV are about 15% at 30° and 20% at 25°. Thus our measurement is precise enough to demonstrate their importance. We find that our results for $d\sigma/d\Omega_1 d\Omega_2$ are consistent with the Coulomb-corrected calculations at 25° and nearly consistent at 30°.

We also obtained the photon angular distributions, $d\sigma/d\Omega_1 d\Omega_2 d\theta_\gamma$. However, because the counter solid angles were chosen to emphasize the bremsstrahlung counting rate (and hence the precision of the integrated cross-section measurement), the kinematic determination of the photon angle was uncertain to about 30°. Consequently the photon angular distributions we obtained are very much smoothed out and cannot be used to directly confront the theoretically predicted shapes. There-

fore these data are a secondary result of the measurement.

In Sec. II we discuss the general problems encountered in performing the measurement, and in Sec. III we present the methods employed to solve these problems. Section IV contains the data analysis and results. A discussion of these results is given in Sec. V.

II. GENERAL CONSIDERATIONS

A. Experimental Problems

The major problems that had to be surmounted in this experiment resulted from the very low PPB cross section ($\sim 1 \mu\text{b}/\text{sr}^2$) which we were measuring in the presence of the relatively high p - p elastic cross section ($\sim 10^5 \mu\text{b}/\text{sr}$). As mentioned above, both final-state protons were detected in coincidence at approximately equal angles on either side of the beam. In order to accumulate PPB data at a sufficient counting rate without an excessive background from accidental coincidences, both the fraction of elastically scattered protons degraded into the PPB energy region and the coincidence resolving time had to be minimized. In addition, because of the high elastic proton counting rate, we had to devise a means to eliminate the pileup distortion of the proton energy pulses. The major experimental effort, discussed in Sec. III, was spent in solving these three problems.

B. Kinematics

The kinematic details of the PPB final state have been discussed by a number of authors.^{3,4} We shall give only the main results here. Plotting E_1 versus E_2 for fixed proton angles, the locus of kinematically allowed proton energies lies on a ring, and each point of the ring corresponds to a unique pair of photon angles, θ_γ and ϕ_γ . If the proton polar angles θ_1 and θ_2 (Fig. 1) are held constant and the noncoplanarity angle ϕ is varied, a family of rings results, the largest ring corresponding to coplanar protons (Fig. 2).

In general, the precise measurement of the energies and polar angles of both of the protons is sufficient to calculate the photon energy and angles together with the noncoplanarity angle ϕ . (One of the proton azimuthal angles is defined to be 180° as in Fig. 1.) However, the allowed proton energies change rapidly with both θ_p and ϕ_p , as is shown in Figs. 2 and 3. Thus if the proton counters have angular acceptances of a few degrees, it is only possible to determine the photon energies and angles approximately.

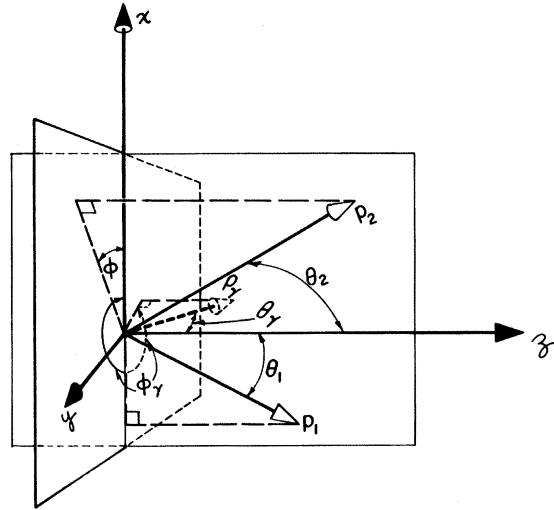


FIG. 1. Diagram of geometrical definitions used. The beam axis is the z axis; \vec{P}_1 defines the x - z plane. Then ϕ is the angle between the x axis and the projection of \vec{P}_2 on the x - y plane.

III. EXPERIMENTAL SOLUTIONS

A. Accidental Coincidences

The proton beam from the University of Washington three-stage Van de Graaff accelerator impinged on a gas target designed especially to minimize the background from degraded particles in the spectrum of scattered protons. The outgoing particles were detected by counter telescopes

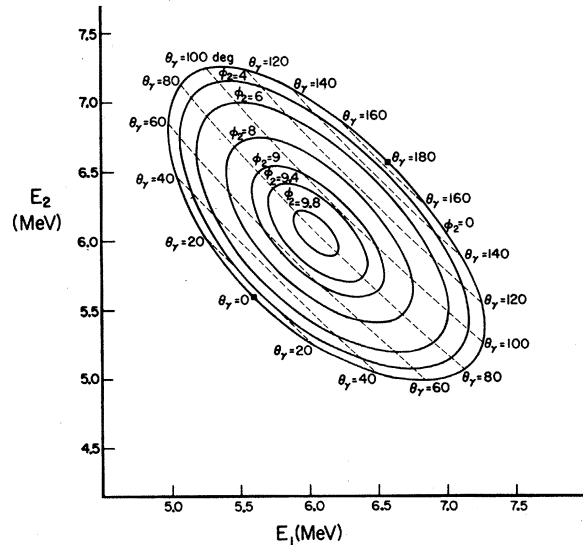


FIG. 2. Plot of various kinematic loci for PPB for $\theta_1 = \theta_2 = 25^\circ$ with 20-MeV incident proton energy. The dashed lines give the loci of points with equal θ_γ . The values of ϕ are shown on the figure.

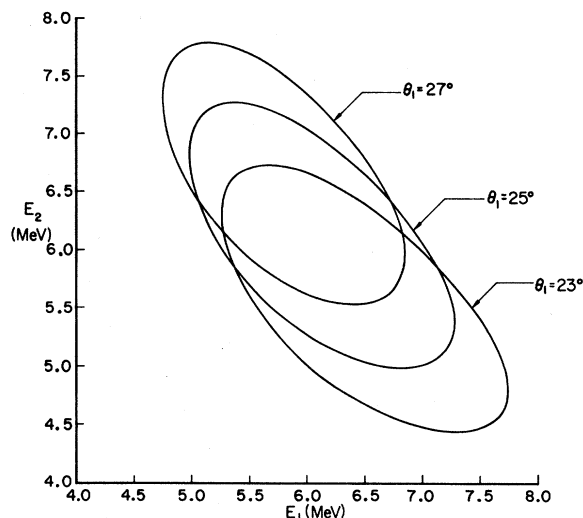


FIG. 3. Plot of various kinematic loci for PPB for $\theta_2 = 25^\circ$ and $\phi = 0$ and for 20-MeV incident proton energy.

whose slit systems were likewise designed to minimize this background.

In tests with a cylindrical gas target we found that a large fraction of the degraded spectrum was due to particles scattered through small angles at the entrance foil of the gas target. These particles were scattered off the slit nearest the target into the detector. To reduce the flux hitting this slit, we designed a gas cell (Fig. 4) with an entrance foil 5.5 in. upstream from the target center. The beam was focused through apertures upstream from the entrance foil so that the beam center position was determined to within about 0.02 in. The beam width was less than 0.08 in. The details of the gas target and beam collimation system are given in work of Storm.⁹

The counter systems (Fig. 5) used in conjunction with this gas cell had nickel slits with rounded edges. The relevant dimensions of the counter slit system appear in Table I. With this slit sys-

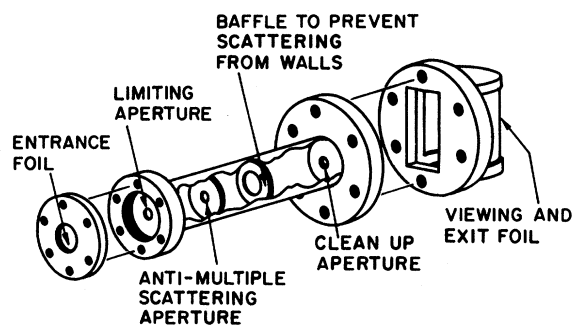


FIG. 4. An exploded view of the gas target. The body and beam-limiting apertures are brass, the baffle is aluminum, and the foils are 1×10^{-4} -in.-thick heat-treated Havar.

tem and the gas target described above, the elastic proton spectrum had an approximately energy-independent tail that was only $0.4\% \text{ MeV}^{-1}$ of the elastic peak. This tail was sufficiently small so that the accidental coincidence rate was not the single limiting factor on the allowable single-counter rates.

B. Particle Identification

The problem of eliminating background due to neutrons and γ rays was solved by using ΔE - E particle-identification systems consisting of two silicon surface-barrier detectors 100 and 700 μ thick, respectively. A third 2-mm-thick lithium-drifted detector was mounted behind the first two. The thicknesses were chosen so the PPB protons would stop in the second detector, while elastic protons would stop in the third which functioned in an anticoincidence mode as described below.

C. Coincidence Determination

The fast timing was accomplished via a time-to-amplitude converter (TAC) which was started by one counter and stopped by the other. The TAC was triggered by signals from the two 700- μ "E" detectors only, since the fast signals from the third detector were used in an anticoincidence mode. Thus the TAC was not triggered by elastically scattered protons. Rather than setting a window on the TAC output to determine prompt- and delayed-coincident events, we fed the TAC signal into an on-line computer which was gated by the output of a coincidence between the E signals. This gating coincidence resolving time was about 80 nsec. The electronics system is diagrammed in Fig. 6.

In order to determine the energy walk of the TAC output corresponding to true coincidences, we calibrated the TAC spectrum in the following way. Us-

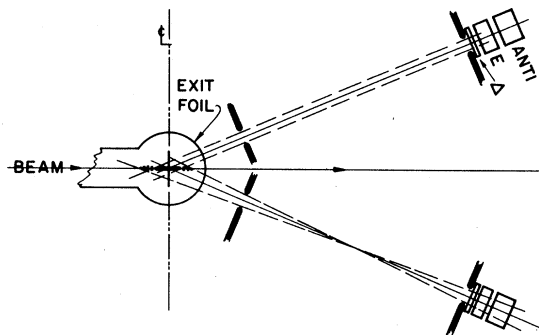


FIG. 5. Counter and slit geometry. The detectors are not drawn to scale. The heavy solid line represents the fully viewed portion of the target volume, and the dashed lines represent the partially viewed portion. The dimensions are the same for both counter systems.

ing coincident elastic events which were detected for various incident energies and detector angles, we fitted a seven-parameter function to the measured variation of TAC amplitude with proton energy. Thus the deviation between the TAC amplitude for any given event and the predicted value for a coincident event with the same proton energy was used to determine the timing. We were able to improve the acceptance interval for prompt-coincident events from 25 to 5 nsec by this procedure. Figure 7 shows the results of this timing procedure. Possible shifts in timing were monitored by daily elastic scattering checks, which showed no instability greater than $\frac{1}{3}$ nsec.

D. Pileup Rejection

Pileup rejection was accomplished in two ways. Analog suppression of the elastic pulses was accomplished by adding the inverted preamplifier pulses of the antidetector to the preamplifier pulses of the ΔE and E detectors before the shaping amplifiers. The gain of the antisignals was adjusted so that a minimum pulse resulted from an elastically scattered proton.

In addition to the analog suppression of the elastic proton signals, we used a pileup rejection gate to eliminate pileup of PPB counts with that part of the elastic proton signal remaining after cancella-

tion. This gate, on the output of the 80-nsec coincidence, was closed for 2.5 μ sec whenever there was an elastic proton in either counter, thus preventing a gate for the entire system.

The combined analog suppression and pileup rejection gate enabled us to maintain an energy resolution of about 70 keV in the presence of 3×10^4 elastic counts/sec in each counter. Without these protective systems the energy resolution would have been several hundred keV.

E. Energy Analysis, Dead Time, and Gain Shifts

The energy analysis was accomplished by digitally adding the signals from the first two detectors in the computer to obtain the particles' energy. The energy measured during the time calibration was also used for the energy calibration. A pulser, whose rate was kept proportional to the PPB rate by triggering with the beam-current integrator, was used to monitor gain shifts and system dead time, which ran between 10 and 15% due to the closing of the pileup rejection gate.

IV. DATA ANALYSIS AND RESULTS

A. General Data Reduction

During the run the four detector energies and the TAC signal for each coincident event were

TABLE I. Experimental geometry.

	Measurement at $\theta_1 = \theta_2 = 25^\circ$	Measurement at $\theta_1 = \theta_2 = 30^\circ$
Front slit to target center	2.000 in.	2.000 in.
Back slit to target center	8.000 in.	10.000 in.
Slit width	0.300 in.	0.375 in.
Fully illuminated target length	0.71 in.	0.75 in.
Partially illuminated length	0.47 in.	0.37 in.
Polar angular acceptance of detector from target center	2.15°	2.15°
Maximum polar angular acceptance including target length	5.72°	5.36°
Maximum vertical aperture	0.675 in.	0.675 in.
Average vertical aperture ^a	0.653 in.	0.638 in.
ϕ_{\max}	9.8°	6.7°
Maximum ϕ detectable	12.55°	8.28°
Solid angle	2.99×10^{-3} sr	2.25×10^{-3} sr
Target cell exit-window radius	0.75 in.	0.75 in.
Target cell exit-window height	2.25 in.	2.25 in.

^a Because the aperture was made by placing two slit jaws in front of a round hole, the boundaries of the top and bottom of the aperture were arcs of a circle. This circle had a diameter equal to the "maximum vertical aperture," and therefore the average height of the aperture was somewhat smaller than this diameter.

stored in an on-line computer and were written on magnetic tape for later analysis. The data on tape were reduced using standard particle-identification techniques and timing criteria which were optimized with the energy-dependent timing scheme described above. These techniques were checked by reducing the elastic proton data (from the calibration runs) and requiring that less than 1% of these events be rejected by timing or particle-identification failures.

This data reduction procedure produced two-dimensional spectra corresponding to both prompt- and delayed-coincidence events. The prompt-coincidence interval (t_p) was set in the computer on the basis of the energy-time calibration. The "80-nsec" coincidence time included the time range $t_p + t_d$, where t_d was the time allotted for the collection of delayed coincidences. The accidental coincidences were then obtained by multiplying the delayed-coincidence spectrum by t_p/t_d which had a value of about 0.1. Prompt- and delayed-coincidence spectra are shown in Fig. 8. The ratio of true to accidental coincidences in the PPB energy region was 1.5 for the 25° data and 11 for the 30° data.

Some results of the accidentals' subtraction are illustrated in Fig. 9. This figure shows that the remaining background outside the energy regions

for PPB and deuteron breakup is small. In all cases but one the total number of counts in this background region gave no statistically significant net counts. In this one run ($\theta_1 = 25^\circ$, $\theta_2 = 27.5^\circ$) there were 27 ± 13 net counts, which would imply a 7-count background in the PPB region, assuming an energy-independent background. A careful search for the cause of this anomaly discounted errors in accidental-background subtraction or background from reactions on impurities. Therefore, in the absence of an explanation for its origin, we did not subtract the 7 counts from the 110 PPB counts, but included an additional 6% uncertainty in that data.

B. Absolute-Cross-Section Determination

The absolute cross section, with the exception of the data at $\theta_1 = \theta_2 = 30^\circ$, was determined from the number of coincidence counts, the gas pressure and temperature, the counter geometry, and the integrated beam current. These quantities contributed an over-all uncertainty of 6% to the cross section. The details of the cross-section determination are straightforward and are discussed elsewhere.⁹ Because the beam diameter (less than 0.08 in.) was very small, finite-beam-width corrections were unnecessary.

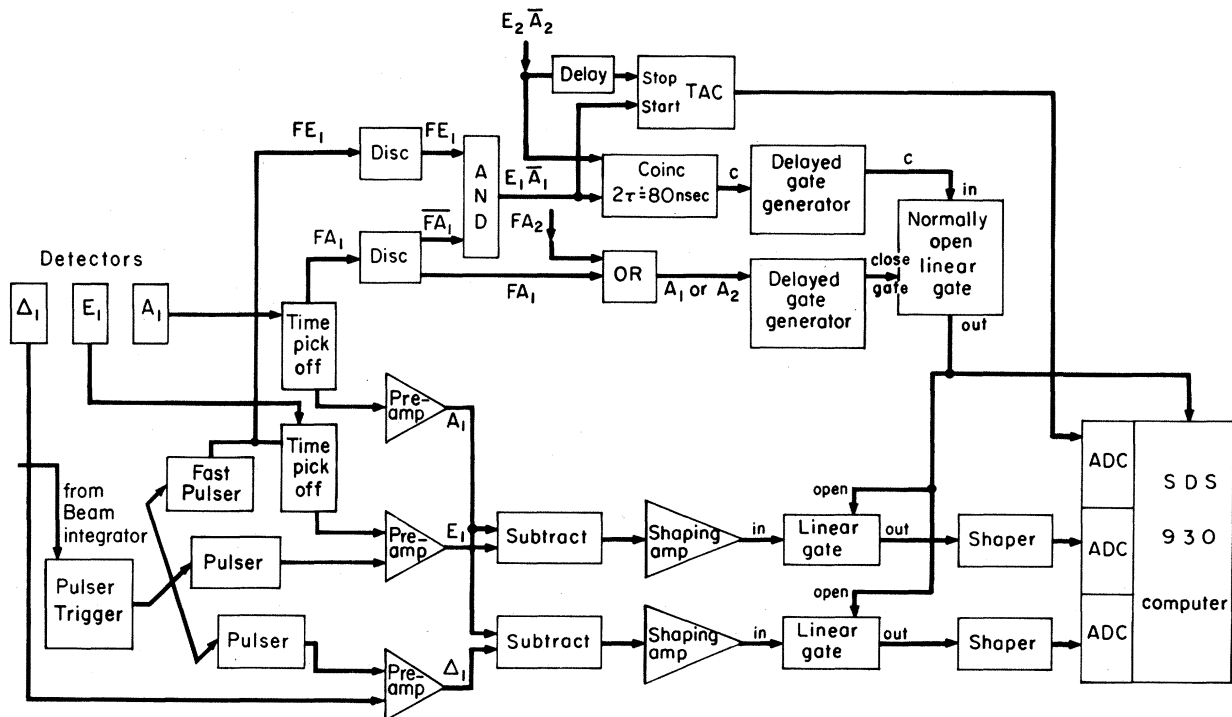


FIG. 6. Simplified electronics diagram. The components that appear for the signals from counter 1 are repeated for counter 2, but are not shown. The two delayed-gate generators and the normally open linear gate constitute the pileup rejection system, with the A_1 or A_2 signal blocking any coincidence signals, C , appearing close in time.

For the data taken at $\theta_1 = \theta_2 = 30^\circ$ the beam-current integration system failed so we had to determine this cross section by normalizing to the single-counter elastic counts. The elastic cross section was obtained from other 30° runs in which the beam-current integrator was working. The cross section obtained agreed to within 4% of the elastic cross section measured at 19.8 MeV.¹⁰ Furthermore, the two counters' rates agreed to within 2% in all runs.

C. Integrated Cross Section, $d\sigma/d\Omega_1 d\Omega_2$

The cross sections resulting from summing all the counts in the kinematically allowed regions for PPB represent an average over the angular acceptances of the counters. The PPB cross section, $d\sigma/d\Omega_1 d\Omega_2$, changes little over the counters' included polar angles. However, the change with azimuthal angle is considerable and important, since the counters subtended the entire kinematically allowed proton azimuthal angle. Neverthe-

less, the correction to the coplanar ($\phi = 0$) cross section can be deduced from the geometrical detection efficiency and from an assumed form for the PPB ϕ dependence. We used the calculations of Drechsel and Maximov^{4,11} for the ϕ dependence and calculated a correction factor k , defined by

$$k = \frac{(d\sigma/d\Omega_1 d\Omega_2)|_{\phi=0}}{\langle d\sigma/d\Omega_1 d\Omega_2 \rangle},$$

where the quantity in the denominator corresponds to the measured result. (These calculations for the ϕ dependence have recently been experimentally verified for 64.4-MeV incident energy and 30° proton angles.²) We found for the geometry for $\theta_1 = \theta_2 = 25^\circ$, $k = 1.137$, while for $\theta_1 = \theta_2 = 30^\circ$, $k = 1.135$. These factors are close to 1 because the geometrical efficiency decreases linearly with ϕ and because the PPB cross section is approximately constant for $\phi < \frac{1}{3}\phi_{\max}$, falling off as ϕ increases. Consequently k is not sensitive to the precise form of the decrease and should be fairly model-independent.

The cross sections and correction factors are given in Table II. Since the polar angular dependence is calculated to be small,⁴⁻⁶ we have combined the data at $\theta_1 = 27.5^\circ$ and $\theta_2 = 25^\circ$, with $\theta_1 = \theta_2 = 25^\circ$ value.

D. Photon Angular Distribution

For our counter geometry, $\Delta\phi$ included the entire azimuthal kinematic range and $\Delta\theta$ spanned several degrees. Consequently, for each event we could only determine a photon probability distribution (f) in θ_γ . The calculation of this probability distribution $f(\theta_\gamma, E_1, E_2)$ is discussed in detail in the Appendix. It depends on the geometrical detection efficiencies and involves a transformation from the final-state kinematic variables E_1 and E_2 to θ_2 and ϕ . This transformation enables us to use the accurate determination of E_1 and E_2 to obtain an approximate value for θ_γ , since θ_γ is kinematically determined by E_1 , E_2 , θ_1 , and θ_2 . The probability distribution had an average full width at half maximum of about 24° for the 25° data and 30° for the 30° data. (The actual width and shape of f varied with the proton energies. For some events the interval containing most of the area under f was smaller than 20° while for a few events it was as large as 35° .) The histograms for the quantities $\langle d\sigma/d\Omega_1 d\Omega_2 d\theta_\gamma \rangle$, averaged over $\Delta\phi$ and $\Delta\theta$, were determined from this probability distribution and are shown in Fig. 10.

V. DISCUSSION OF RESULTS

The current calculations⁴⁻⁶ for $d\sigma/d\Omega_1 d\Omega_2$ are in general agreement with our results. (These calcu-

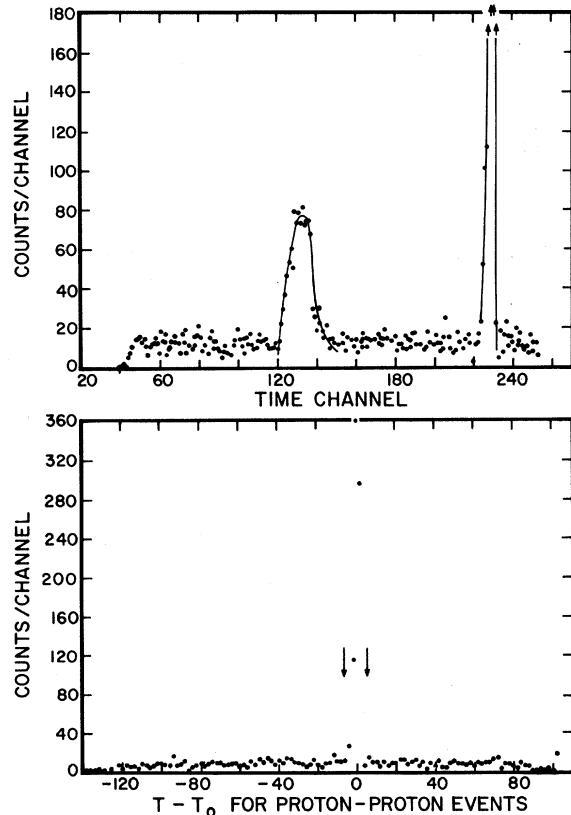


FIG. 7. Typical raw and corrected time spectra. The top graph shows the TAC spectrum for all events, including the pulser. The bottom graph shows the spectrum of deviations from the calculated time T_0 for prompt events. Only proton events are included. The arrows indicate the acceptance interval.

lations explicitly include OES effects.) The cross sections calculated by Marker and Signell⁵ are in excellent agreement with the 25° data and are only somewhat more than one standard deviation larger than the 30° measurement. These calculations include the Coulomb force in an on-shell approximation.⁵ The importance of these Coulomb corrections for 20-MeV incident energy is evident as shown in Table II.

Although the OES effects are larger at 25° than at 30°, the calculated cross section remains insensitive to the choice of the two-proton potential. Marker and Signell⁵ have pointed out that this is not a result of the independence of the PPB amplitude from OES effects, but rather arises from the fact that some terms in the amplitude have OES behavior which cancels the OES behavior of other terms. This cancellation is equally effective at 25° as at 30°.

Maximon has calculated¹¹ photon angular distributions for various ϕ and for θ_1 and θ_2 appropriate to this experiment. We have presented these calculations, averaged over the experimental geometry, along with the data in Fig. 10. To facilitate a comparison of shapes, the theoretical photon angular distributions in Fig. 10 have been normalized to give the same values for $d\sigma/d\Omega_1 d\Omega_2$ as the measured ones. The effect of folding the experimental photon angular resolution into the calculations is also shown. The averaged theory shows the two-bump angular distribution which many authors⁴⁻⁸ have shown to be characteristic of the photon angular distributions for $\phi=0$ and for equal proton polar angles. There is further a rough forward-backward symmetry about 90°. These characteristics of the γ angular distribution are quite general and stem from the following. The two-proton system has no electric dipole moment in the center of

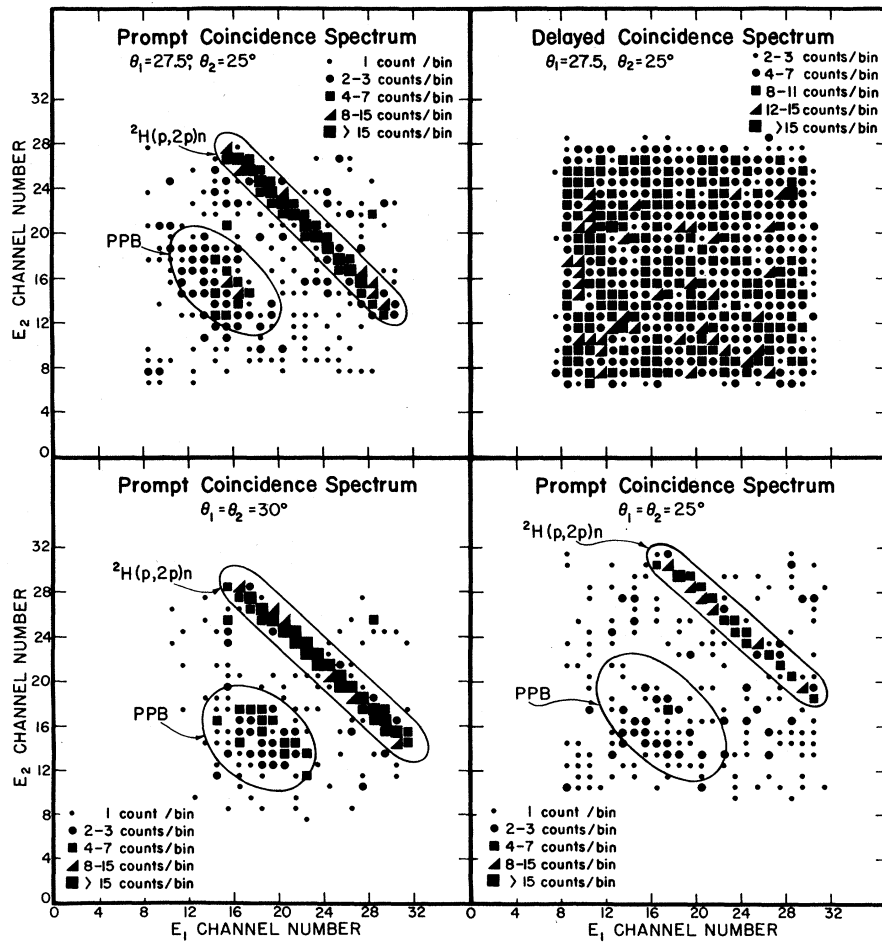


FIG. 8. Some raw spectra. Each spectrum shown is the result of an entire run. The top two panels show spectra of corresponding prompt- and delayed-coincidence data. The bottom panels show prompt-coincidence spectra. In all the prompt spectra the events from PPB as well as from $^2\text{H}(p,2p)n$ show clearly above the background, which is almost entirely due to accidental coincidences. The delayed-coincidence spectrum is typical, and it shows that the accidental background varies slowly with the energy of the detected protons.

TABLE II. Comparison of measured cross sections with theory.

θ (deg)	θ (deg)	$d\sigma/d\Omega_1 d\Omega_2$ ($\mu\text{b}/\text{sr}^2$)	k	$(d\sigma/d\Omega_1 d\Omega_2) _{\phi=0}$ ($\mu\text{b}/\text{sr}^2$)	Theoretical values for $(d\sigma/d\Omega_1 d\Omega_2) _{\phi=0}$ ($\mu\text{b}/\text{sr}^2$)		
					D-M ^a no Coulomb	M-S ^b no Coulomb	M-S ^b with Coulomb
25	25	0.55 ± 0.10	1.137	0.62 ± 0.10	0.81	0.82	0.65
25	25						
Combined with		0.60 ± 0.06	1.137	0.68 ± 0.07			
27.5	25						
30	30	0.61 ± 0.07	1.135	0.69 ± 0.07	0.91	0.93	0.80

^a See Refs. 4 and 11.^b See Ref. 5.

mass. Therefore, since the nuclear scattering at 20 MeV is strongest in the S state, the radiation must involve a change of the two-proton orbital angular momentum from S to D or D to S, depending on whether the radiation follows or precedes the scattering. This yields electric quadrupole radiation. [Magnetic dipole radiation involves transitions between relative P- (or higher) wave states and so is suppressed.] Regardless of the γ multipolarity, however, the angular distribution is constrained to be symmetric about 90° c.m. because of the indistinguishability of the two protons. The transformation from the c.m. to the lab system will introduce some asymmetry about 90° depending upon the proton detection angles and the incident energy.

The measured photon angular distributions (Fig. 10) are in agreement with the theory for the 30° data but are in somewhat poorer agreement at the smaller proton angles. These results in all cases indicate a smooth angular distribution with some predominance of the cross section forward of 90° for the $\theta_1 = \theta_2 = 25^\circ$ and the combined 25–27.5° cases. There is symmetry about 90° for the $\theta_1 = \theta_2 = 30^\circ$ data. Possible experimental causes for the lower cross section at larger θ_γ (corresponding to smaller E_γ) were carefully investigated. The required error in the energy calibration would have had to have been about 500 keV, which is unreasonably large. Since the events in question occurred at about the middle of the counters' energy-acceptance range, counter energy cutoff was also re-

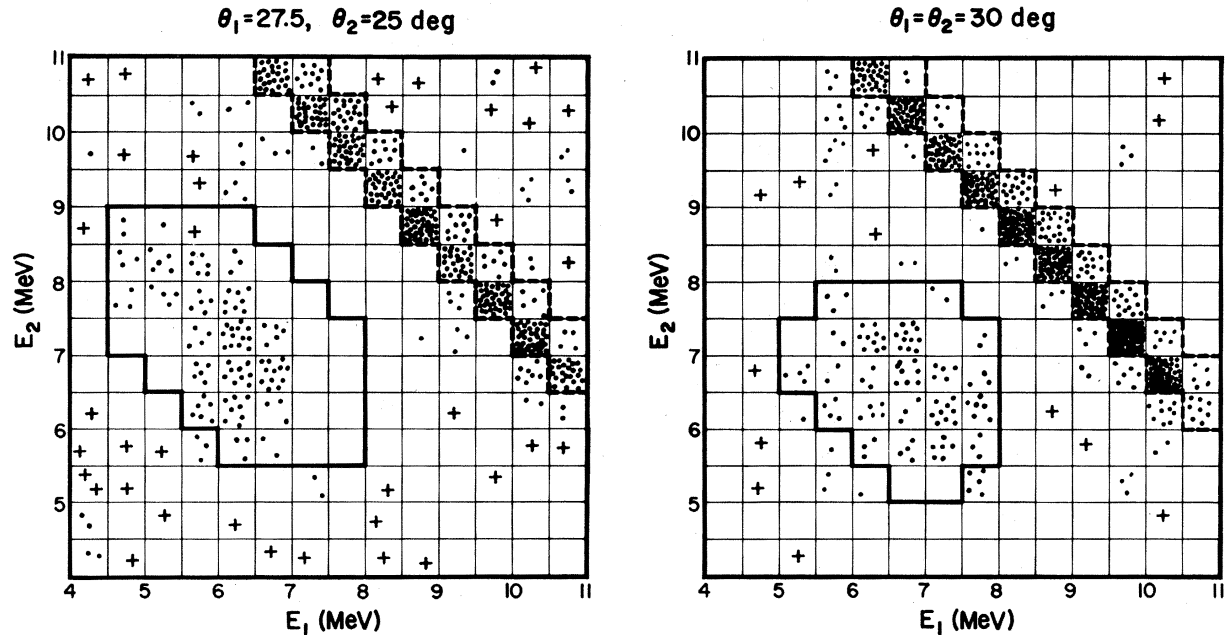


FIG. 9. Rehistogrammed spectra with accidental-coincidence background subtracted. The number of dots per bin is equal to the net counts, rounded to the nearest integer. A cross represents a negative net result. The spectra are from runs at $\theta_1 = \theta_2 = 30^\circ$ and at $\theta_1 = 27.5$ and $\theta_2 = 25.0^\circ$. The PPB regions are outlined by heavy, solid lines. The regions for events from the ${}^2\text{H}(p, 2p)n$ reaction are outlined by heavy dashed lines.

jected. Also, since the effect was present even before background subtraction, we ruled out errors due to background corrections. Thus we believe the discrepancies between the data and the calculations at the smaller proton angles are probably due to the inherently poor photon angular determination and are not significant. Other experiments^{1,2} indicate that for azimuthal angles near

$\phi=0$, the photon angular distributions have the symmetric quadrupole shape predicted by theory. For large ϕ , however, there has been only one published measurement of the angular distribution and that was for 158 MeV (Gottschalk, Schlaer, and Wang³). More such measurements would be interesting, though difficult.

ACKNOWLEDGMENTS

We would like to thank Professor I. Halpern for his advice during the running of the experiment and for his careful reading of the manuscript. We express our gratitude to Professor E. M. Henley and Dr. F. Richards for many valuable theoretical discussions. Finally, we are indebted to both Professor P. Signell and Professor L. C. Maximon for their calculations of the PPB cross sections and to D. R. Brown, K. G. Nair, and P. A. Russo who helped with the data taking.

APPENDIX: DETERMINATION OF θ_γ

The large uncertainty with which we determined the proton angular variables forced us to adopt a somewhat more analytic method to extract the photon angular distributions than is usually employed. In general, five independent variables are sufficient to determine the kinematic solutions for any PPB event. We measured two of these variables, E_1 and E_2 , with sufficient accuracy so that their uncertainty contributed little variation to θ_γ . (A third variable, ϕ_1 , was defined to be π as in Fig. 1. This variable is arbitrary because of the over-all azimuthal symmetry.) We may therefore relate the number of measured counts with proton energies E_1 and E_2 , $\langle dN/dE_1 dE_2 d\alpha d\beta d\gamma \rangle_{\alpha\beta\gamma}$, to the differential cross section averaged over the experimental acceptance for any three kinematic angle variables, α , β , and γ . For convenience we choose to express this as an average over Ω_1 and θ_γ , where Ω_1 is the solid-angle variable for particle 1:

$$\left\langle \frac{dN}{dE_1 dE_2 d\Omega_1 d\theta_\gamma} \right\rangle_{\Omega_1 \theta_\gamma} \propto \int \frac{d\sigma}{dE_1 dE_2 d\Omega_1 d\theta_\gamma} \times \epsilon_T(\theta_1 \theta_2) \epsilon_p(\phi) d\Omega_1 d\theta_\gamma, \quad (1)$$

where θ_2 and ϕ are given as functions of θ_1 , θ_γ , E_1 , and E_2 by momentum and energy conservation. The detection efficiencies $\epsilon_T(\theta_1 \theta_2)$ and $\epsilon_p(\phi)$ are obtained by considering the geometrical fractions of the counters and target available for detecting events with pairs of polar angles θ_1 and θ_2 and with the noncoplanarity angle ϕ , respectively.⁹

We now transform the cross section in (1) to the

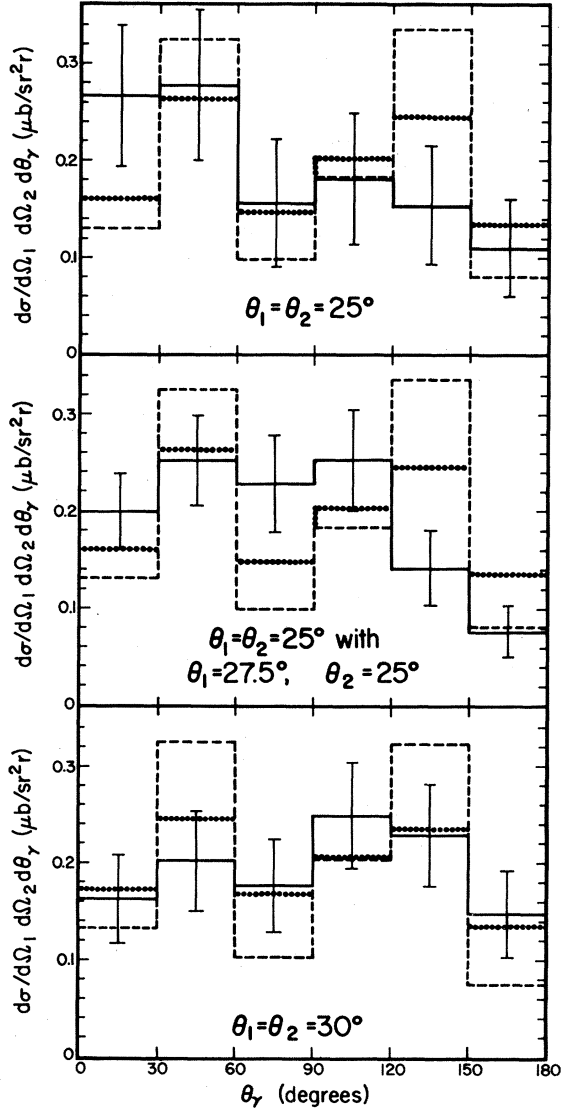


FIG. 10. Histograms of photon angular distributions, averaged over the proton counters' angular acceptances. The proton counter angles are given on the graphs. The averaged theoretical calculations of Drechsel and Maximon (Ref. 11) normalized to the measured values of $d\sigma/d\Omega_1 d\Omega_2$ are shown by dashed lines. These calculations, smeared out by the average experimental resolution, are shown by dotted lines. The calculations for $\theta_1 = \theta_2 = 25^\circ$ are also shown on the plot of the combined 27.5-25° and 25-25° data.

cross section calculated by most theorists, $d\sigma/d\Omega_1 d\Omega_2 d\theta_\gamma$, using the Jacobian (J) for the transformation giving $\cos\theta_2$ and ϕ in terms of E_1 and E_2 . Employing conservation of momentum (P) along the beam and perpendicular to the beam, we obtain

$$\cos\theta_2 = (P_0 - P_1 \cos\theta_1 - P_\gamma \cos\theta_\gamma)/P_2,$$

and

$$\cos\phi = \frac{P_\gamma^2 \sin^2\theta_\gamma - P_1^2 \sin^2\theta_1 - P_2^2 \sin^2\theta_2}{2P_1 P_2 \sin\theta_1 \sin\theta_2}, \quad (2)$$

respectively.

Then the Jacobian is obtained by calculating the determinant

$$J = \begin{vmatrix} d\phi/dE_1 & d(\cos\theta_2)/dE_1 \\ d\phi/dE_2 & d(\cos\theta_2)/dE_2 \end{vmatrix}.$$

The result is complicated, but when the protons are treated nonrelativistically, we obtain (with m as the proton mass)

$$J = \frac{m^2}{P_1 P_2^2 \sin\theta_1 \sin\theta_2 \sin\phi} \left| \frac{\sin^2\theta_2 \cos\theta_1}{P_1} - \frac{\sin^2\theta_1 \cos\theta_2}{P_2} + \frac{\cos\theta_2}{mc} (\sin^2\theta_1 - \sin^2\theta_2) + \sin\theta_1 \sin\theta_2 \cos\phi \right. \\ \left. \times \left[\frac{\cos\theta_1}{P_2} - \frac{\cos\theta_2}{P_1} - \left(\frac{P_1}{P_2} - \frac{P_2}{P_1} \right) \frac{\cos\theta_\gamma}{mc} \right] \right|,$$

where we have ignored a term proportional to E_γ/mc^2 . The right-hand side of Eq. (1) now becomes

$$\int J \left(\frac{d\sigma}{d\Omega_1 d\Omega_2 d\theta_\gamma} \right) \epsilon_p \epsilon_T d\Omega_1 d\theta_\gamma. \quad (3)$$

The integral over $d\Omega_1$ may be approximated by noting that the variation of $d\sigma/d\Omega_1 d\Omega_2 d\theta_\gamma$ with θ_1 over the limited angular acceptance of the counters is small and may be ignored. A further approximation involves treating the ϕ dependence of $d\sigma/d\Omega_1 d\Omega_2 d\theta_\gamma$ with an appropriate average over ϕ . Thus the expression in (3) is written as

$$\int \langle d\sigma/d\Omega_1 d\Omega_2 d\theta_\gamma \rangle_\phi f(\theta_\gamma, E_1, E_2) d\theta_\gamma, \quad (4)$$

where

$$f(\theta_\gamma, E_1, E_2) = \int J \epsilon_T(\theta_1, \theta_2) \epsilon_p(\phi) d\Omega_1,$$

and ϕ and θ_2 are expressed as functions of E_1 , E_2 , θ_1 , and θ_γ . Now the integral in (4) cannot be evaluated without a knowledge of $\langle d\sigma/d\Omega_1 d\Omega_2 d\theta_\gamma \rangle_\phi$ for each pair of proton energies. However, the probable range for θ_γ corresponding to an event with given proton energies can be determined by calculating f . This range was found to increase with increasing θ_γ , and varied from about 21 to 33° for the 25° proton detection angles and from 24 to 38° for the 30° proton angles. Thus we calculated a histogram for the photon angular distribution, dividing the counts among the histogram bins as the calculation of f dictated.

The evaluation of f was done numerically and, except for the singularities in J at $\phi = 0$, this calculation was straightforward. To evaluate the contribution from the regions near $\phi(\theta_1, \theta_\gamma, E_1, E_2) = 0$, we defined θ_{10} by $\phi(\theta_{10}, \theta_\gamma, E_1, E_2) = 0$ and used Eq. (2) for $\cos\phi$ to give

$$\int_{\theta_{10}}^{\theta_{10} + \Delta} \frac{d\theta_1}{\sin\phi} \\ \approx 2 \left[\left| \Delta \frac{d}{d\theta_1} (1 - \cos^2\phi) \right| \right]^{1/2} \\ = \left\{ \left| 2\Delta \left[\frac{P_1}{P_2} \frac{\sin(\theta_2 - \theta_1)}{\sin^2\theta_2} + \frac{\sin(\theta_2 - \theta_1)}{\sin\theta_2 \sin\theta_1} \right] \right| \right\}^{1/2},$$

where we have expanded $\sin\phi$ to first order in Δ in order to do the integral. In the region in which the singularities' contribution to the integral was evaluated we assumed that the other factors in the integrand were constant. This assumption was estimated to be valid to within 10% when Δ was one degree.

The quantities $\epsilon_T(\theta_1, \theta_2)$ and $\epsilon_p(\phi)$ produced the major restrictions on the region in which f was nonnegligible. In fact histograms calculated with the assumption that J was a constant differed little from those calculated with the inclusion of the correct form for J (except in the bins for photon angle nearest 0 or 180°). The major effect of setting J constant was to diminish the cross section in those bins corresponding to the extreme values of θ_γ .

*Work supported in part by the U. S. Atomic Energy Commission.

†Now at Columbia University, Nevis Laboratories,

Irvington, New York 10533.

¹F. Sannes, J. Trischuk, and D. G. Stairs, Phys. Rev. Letters 21, 1474 (1968).

²D. O. Galde, M. L. Halbert, C. A. Ludemann, and A. van der Woude, *Phys. Rev. Letters* **25**, 1581 (1970); M. L. Halbert, D. L. Mason, and L. C. Northcliffe, *Phys. Rev.* **168**, 1130 (1968).

³A. Niiler, C. Joseph, V. Valkovic, R. Spiger, T. Canada, S. T. Emerson, J. Sandler, and G. C. Phillips, *Phys. Rev.* **178**, 1621 (1969); E. A. Silverstein and K. G. Kibler, *Phys. Rev. Letters* **21**, 922 (1968); J. Sanada, M. Yamanouchi, T. Tagishi, Y. Nojiri, K. Kondo, S. Kobayashi, K. Nagamine, N. Ryu, H. Hasai, M. Nishi, M. Seki, and D. C. Worth, *Progr. Theoret. Phys. (Kyoto)* **39**, 853 (1968); B. Gottschalk, W. J. Schlaer, and K. H. Wang, *Nucl. Phys. A* **94**, 491 (1967); K. W. Rothe, P. F. M. Koehler, and E. M. Thorndike, *Phys. Rev.* **157**, 1247 (1967); R. E. Warner, *Can. J. Phys.* **44**, 1225 (1966); J. V. Javanovich, L. G. Greeniaus, J. McKeown, T. W. Miller, D. G. Peterson, W. F. Prickett, K. F. Suen, and J. C. Thompson, *Phys. Rev. Letters* **26**, 277 (1971); D. L. Mason, M. L. Halbert, A. van der Woude, and L. C. Northcliffe, *Phys. Rev.* **179**, 940 (1969), and references

contained therein.

⁴D. Drechsel and L. C. Maximon, *Ann. Phys. (N.Y.)* **49**, 403 (1968).

⁵D. Marker and P. Signell, *Phys. Rev.* **185**, 1286 (1969); P. Signell, in *Advances in Nuclear Physics* (Plenum, New York, 1968), Vol II; and P. Signell, private communication.

⁶V. R. Brown, *Phys. Rev.* **177**, 1498 (1969).

⁷J. H. McGuire, A. H. Cromer, and M. I. Sobel, *Phys. Rev.* **179**, 948 (1969), and references contained therein.

⁸E. M. Nyman, *Phys. Rev.* **170**, 1628 (1968); W. A. Pearce, W. A. Gale, and I. M. Duck, *Nucl. Phys. B* **3**, 241 (1967); F. E. Low, *Phys. Rev.* **110**, 974 (1958); L. Heller, *ibid.* **174**, 1580 (1968); **180**, 1616 (1969); and M. K. Liou, *Phys. Rev. C* **2**, 131 (1970).

⁹D. W. Storm, Ph.D. thesis, University of Washington, 1970 (unpublished).

¹⁰J. W. Burkig, J. R. Richardson, and G. E. Schrank, *Phys. Rev.* **113**, 290 (1959).

¹¹L. C. Maximon, private communication.

PHYSICAL REVIEW C

VOLUME 4, NUMBER 5

NOVEMBER 1971

Nuclear Deexcitation γ Rays in ^{14}N , ^{14}C , and ^{15}N Following π^- Capture on $^{16}\text{O}^+$

W. J. Kossler and H. O. Funsten

College of William and Mary, Williamsburg, Virginia 23185

and

B. A. MacDonald

Virginia Polytechnic Institute and State University, Blacksburg, Virginia 24061

and

W. F. Lankford

George Mason College, Fairfax, Virginia 22030

(Received 30 June 1971)

Negative pions produced by the National Aeronautics and Space Administration Space Radiation Effects Laboratory cyclotron were stopped in water and the nuclear deexcitation γ rays observed. γ rays from ^{14}N , ^{15}N , and ^{14}C were identified, and yields to particular states in these nuclei obtained. A prominent γ -ray peak in our spectra was from the 3.945-MeV 1^+ state in ^{14}N which was formed with a rate of 1.8% per stopped pion. The Doppler-broadened line shape of the decay γ ray for this state was analyzed to obtain the momentum distribution of the recoiling ^{14}N nucleus. This momentum distribution is compared with momentum distributions obtained by related experiments, and to theoretical predictions. Yields to various states are presented and discussed.

I. INTRODUCTION

Several years ago it was pointed out by Ericson¹ that π^- capture is a useful probe of nuclear structure. The experiment considered here is of a new type using π^- absorption. We have observed nuclear γ rays from states in nuclei left after π^- absorption. We obtain from the relative yields of particular γ rays information on the relative rates for producing the nuclear states which pre-

cede these γ rays. The Doppler-broadened line shapes of some transitions contain implicitly the momentum spectrum of recoiling nuclei and hence the sum-momentum distribution of ejected particles. Since the π^- absorption process proceeds with high probability by ejecting two nucleons,² this momentum distribution is the sum momentum of nucleon pairs. Further, since the level from which the γ ray comes is known, comparison between theoretical predictions and the experimental